Prediction models for wind speed at turbine locations in a wind farm

Knudsen, Torben; Bak, Thomas; Soltani, Mohsen

Published in:
Wind Energy

DOI (link to publication from Publisher):
10.1002/we.491

Publication date:
2011

Document Version
Publisher's PDF, also known as Version of record

WIND ENERGY
Wind Energ. 2011; **14**:877–894
Published online 8 August 2011 in Wiley Online Library (wileyonlinelibrary.com). DOI: 10.1002/we.491

SPECIAL ISSUE PAPER

Prediction models for wind speed at turbine locations in a wind farm

Torben Knudsen, Thomas Bak and Mohsen Soltani

Department of Electronic Systems Automation and Control, Aalborg University, Fredrik Bajers Vej 7, DK-9220 Aalborg, Denmark

ABSTRACT

In wind farms, individual turbines disturb the wind field by generating wakes that influence other turbines in the farm. From a control point of view, there is an interest in dynamic optimization of the balance between fatigue and production, and an understanding of the relationship between turbines manifested through the wind field is hence required. This paper develops models for this relationship. The result is based on two new contributions: the first is related to the estimation of effective wind speeds, which serves as a basis for the second contribution to wind speed prediction models.

Based on standard turbine measurements such as rotor speed and power produced, an effective wind speed, which represents the wind field averaged over the rotor disc, is derived. The effective wind speed estimator is based on a continuous–discrete extended Kalman filter that takes advantage of nonlinear time varying turbulence models. The estimator includes a nonlinear time varying wind speed model, which compared with literature results in an adaptive filter. Given the estimated effective wind speed, it is possible to establish wind speed prediction models by system identification. As the prediction models are based on the result related to effective wind speed, it is possible to predict wind speeds at neighboring turbines, with a separation of over 700 m, up to 1 min ahead reducing the error by 30% compared with a persistence method. The methodological results are demonstrated on data from an off-shore wind farm.

KEYWORDS

wind farm; wind speed prediction; effective wind speed estimation; extended Kalman filter; system identification

Correspondence

Torben Knudsen, Department of Electronic Systems Automation and Control, Aalborg University, Fredrik Bajers Vej 7, DK-9220 Aalborg, Denmark.
E-mail: tk@es.aau.dk

Received 1 December 2009; Revised 10 September 2010; Accepted 12 May 2011

NOMENCLATURE

β	Blade pitch angle
Δ	Discrete Dirac delta function
diag	Diagonal matrix with given elements
$\hat{}$	Estimate or prediction
$\hat{x}(t\|t_k)$	State estimate at time t based on measurement including t_k
$\hat{x}(t_k^+)$	State estimate at time t_k based on measurement including t_k
$\hat{x}(t_k^-)$	State estimate at time t_k based on measurement including t_{k-1}
$\in \mathrm{ID}(0, \sigma^2)$	Independent distributed (white noise) with mean 0 and standard deviation σ
$\|$	Conditioned upon, e.g., $\mathrm{E}(x\|y)$ conditional mean of x given y
ω	Frequency [rad s^{-1}]
ω_m	Rotor speed measurement
ω_r	Rotor speed
ψ_0	Constant term
ρ	Air density
σ_K	Turbulence standard deviation from Kaimal spectrum

σ_{v_t}	Turbulence standard deviation from state space model
a	Wind speed—dynamic parameter
$A, B, C, D, F(q^{-1})$	Transfer function polynomials
A_r	Rotor area
C_p	Rotor efficiency
C_t	Rotor thrust coefficient
d	Distance between locations
d_n	Nacelle displacement
d_t	Tower damping constant
f	Frequency [Hz]
$f(x,u)$	State transition function
F, B, H, D	State space model parameters
F_r	Axial rotor force
$f_{p,K}$	Peak frequency from Kaimal spectrum
f_{p,v_t}	Peak frequency from state space model
$G, H(q^{-1})$	Transfer functions
$h(x,u)$	Output function
I_r	Equivalent inertia
K	Kalman gain
k_t	Tower spring constant
L	Turbulence length scale parameter
M_n	Equivalent nacelle mass
N	Number of samples
n_i	Continuous time white noise
P	State estimation error covariance
P_g	Generator power
Q	Incremental process noise covariance
q^{-1}	Back shift operator
R	Measurement noise covariance
R_r	Rotor radius
S_U	Turbulence spectrum
T_g	Generator torque
t_i	Turbulence intensity
T_l	Torque from losses, e.g., friction
T_r	Rotor torque
u	Input
u_i, u_j	Wind speed at two locations
U_{10}	10 min average wind speed
V	Incremental covariance matrix—wind
v	Measurement noise
v_e	Effective wind speed
v_m	Wind speed—10 min average part
v_n	Nacelle wind speed measurement
v_r	Wind speed—relative to nacelle
v_t	Wind speed—turbulent part
x	State
y	Output
EWS	Effective wind speed
NWS	Nacelle wind speed

1. INTRODUCTION

Control of wind farms can be separated into two levels. The controller serving the demands of the network operator gives a set point for active and reactive power for the whole farm. This set point can be the result of several operational modes: maximum energy production, rate limiting, balancing, frequency control, voltage control or delta control.[1,2] The next level of wind farm control implements a strategy for distributing set points to individual turbines in order to achieve the overall demand. Currently, this is carried out in a simplistic manner where all turbines are essentially treated the same, disregarding

Wind Energ. 2011; **14**:877–894 © 2011 John Wiley & Sons, Ltd.
DOI: 10.1002/we

the local wind field and turbine status. The turbines affect each other through wakes, and given that models that describe this relationship can be established, a dynamic optimization may be performed using methods such as model predictive control[3,4] or decentralized control.[5] The objective of the optimization would be to meet the overall demand in terms of power, at the same time minimizing the load on individual turbines, resulting in an increased efficiency of the plant.

Central to modeling the relationship between turbines in a farm is modeling the wind speed at the turbine locations given the wind speed at upwind turbines. In Sørensen *et al.*,[6(p8)] it is concluded that the prediction of wind speeds from upwind turbines is not useful. Nielsen *et al.*[7] reports useful models for point wind speeds at separation of 300 m but a very weak relation over 600 m. The point speed coherence function[8] supports this observation. These results from the literature suggest that point wind speed cannot be predicted over the distances typical for a wind farm. In Nielsen *et al.*,[7] a specific model for predicting point speeds from measured upwind point speeds was presented. The model includes a stochastic part of autoregressive moving average (ARMA) type and will serve as inspiration for the work presented here.

In this paper, the hypothesis is that *effective wind speed* (EWS),[9,10] which represents the wind field averaged over the rotor disc, may be a more appropriate measurement to serve as a base for prediction models. Previous results on effective wind speed estimation include Van der Hooft and Van Engelen,[11], which is based on a single-inertia noise-free model. A similar approach is taken in Odgaard *et al.*,[12] but the results are not promising. A two-inertia model is used in combination with a Kalman filter (KF) in Østergaard *et al.*,[9] but the solution is sub-optimal. In Qiao *et al.*,[13] a single-inertia model with estimation based on training a Gaussian radial basis function network is presented. The models used are either one or two inertia drivetrain models, and the estimation method is either direct or KF based. The estimate is the drivetrain torque, and this is then translated to wind speed using C_p tables. A problem in this approach is that it does not include a wind model.

The work presented here first sets up a model structure including a wind model for estimating the EWS and then presents a continuous–discrete extended KF. The nonlinear equations are used when possible, and a third-order linearized model otherwise. The result is a filter that allows estimation of the EWS based on 1 s standard wind turbine data. Given estimated effective wind speeds, system identification may be applied to the problem of establishing wind speed prediction models. To demonstrate the efficacy of the proposed combination of EWS estimation and system identification, data from an off-shore wind farm are used.

The remainder of this paper is organized as follows. First, methods to estimate the effective wind speed are presented. Then the measurement data are described. These data are from the Dutch farm 'Offshore Wind Farm Egmond aan Zee' (OWEZ). This is followed by system identification. The result is validated from a system identification perspective, and finally, the prediction performance is compared with the results from the literature and simple standard methods.

2. ESTIMATION OF EFFECTIVE WIND SPEED

Estimation of EWS can be approached as a standard estimation problem[14] based on the underlying wind turbine model.

$$\dot{x} = f(x, u, w) \tag{1a}$$

$$y = h(x, u, v) \tag{1b}$$

where x is the state including the EWS, u is the input, i.e., blade pitch and generator torque or power reference, and w is process noise that drives the wind model. In the output equation, y is the measurement, e.g., of rotor speed and produced power, and v is the measurement noise. In the following, a model of the type (1) will be established.

2.1. Model

In Van der Hooft and Van Engelen,[11] a single-inertia noise-free model is presented (2b) for direct calculation of the rotor torque. The EWS is then calculated from the pitch angle, rotor speed and rotor torque by equation (2c), where the notation *solve* is used because there can be two solutions to the equation.

$$I_r \dot{\omega}_\mathrm{r} = T_\mathrm{r} - T_\mathrm{g} - T_\mathrm{l} \Rightarrow \tag{2a}$$

$$T_\mathrm{r} = I\dot{\omega}_\mathrm{r} + T_\mathrm{g} + T_\mathrm{l}, T_\mathrm{g} = \frac{P_\mathrm{g}}{\omega_\mathrm{r}}, T_\mathrm{l} = c_c + c_f \omega_\mathrm{r} \tag{2b}$$

$$\hat{v}_\mathrm{e} = \arg\underset{v_\mathrm{e}}{\mathrm{solve}}\, T_\mathrm{r}\omega_\mathrm{r} = \frac{1}{2}\rho v_\mathrm{e}^3 A_\mathrm{r} C_p(\lambda, \beta), \lambda = \frac{R_\mathrm{r}\omega_\mathrm{r}}{v_\mathrm{e}} \tag{2c}$$

When selecting the model structure, it is appropriate to include dynamics from the slow frequency and up to some limiting frequency. To this end, the dynamics and typical frequencies for a multimegawatt turbine are listed in Table I.

The data presented here are from the OWEZ farm.[15] It is averaged over 1 s and sampled at 1 s, which means that only frequencies up to 0.5 Hz are seen. As it makes no sense to include frequencies above the Nyquist frequency in the estimation model, the second drivetrain (drivetrain torsion) and 3P can be omitted. Also, 1P is omitted as its influence on speed, and power is very small for turbines with rotors in good balance.

Another phenomenon that potentially could be considered is dynamic inflow. The physics behind dynamical inflow[16] is the time it takes the flow field to become stationary after a pitch change. As a rule of thumb, the associated time constant is $1.5 \times 2R_r/v_m$ or the time it takes to travel 1.5 rotor diameters with the mean wind speed. Preliminary investigations (not included here) on OWEZ data show no sign of this effect.

From the spectra in Figure 7, a peak at 0.26 Hz is seen. This is actually closer to 1P than to the tower frequency around 0.24 Hz. However, especially at higher wind speeds, the tower dynamics is considered to be important. If possible, it will therefore be included. Notice also that, e.g., rotor speed seems damped at frequencies over $3 \cdot 10^{-2}$ Hz, which can be due to the total drivetrain inertia. Another important observation is that the nacelle wind speed (NWS) is a very uncertain measurement for the free wind speed. This is indicated by the flat spectrum for the NWS at high frequencies as the spectrum should decay with exponent $-5/3$.

In conclusion, the single-inertia and tower fore aft dynamics will be included in the estimator model. This model is explained in the following. The state space part (equation (3)) includes the drivetrain (equation (3a)), tower dynamics (equation (3b)) and wind speed model (equations (3c)–(3d)).

$$I_r \dot{\omega}_r = T_r - T_g \tag{3a}$$

$$M_n \ddot{d}_n = F_r - k_t d_n - d_t \dot{d}_n \tag{3b}$$

$$\dot{v}_t = -a(v_m) v_t + n_1 \tag{3c}$$

$$\dot{v}_m = n_2 \tag{3d}$$

$$T_r = \frac{1}{2} \rho v_r^3 A_r C_p(\lambda, \beta) \frac{1}{\omega_r} \tag{3e}$$

$$F_r = \frac{1}{2} \rho v_r^2 A_r C_t(\lambda, \beta) \tag{3f}$$

$$\lambda = \frac{\omega_r R_r}{v_r} \tag{3g}$$

$$T_g = \frac{p}{\mu \omega_r} \tag{3h}$$

$$v_r = v_t + v_m - \dot{d}_n \tag{3i}$$

Table I. Typical frequencies for dynamics in a multimegawatt turbine.

Dynamics	Frequency (Hz)
First drivetrain	0
Dynamic inflow	0.012
Tower	0.240
1P	0.268
3P	0.803
Second drivetrain	1.606

Dynamics inflow is at 10 m s^{-1} and based on 1.5 D rule of thumb.

Wind Energ. 2011; **14**:877–894 © 2011 John Wiley & Sons, Ltd.
DOI: 10.1002/we

The mechanical part of equation (3) is quite standard and discussed in several textbooks.[17,18] The measurement part (4) simply adds white measurement noise to the rotor speed ω_r and the wind speed seen by the nacelle v_r.

$$\omega_m = \omega_r + v_1 \tag{4a}$$

$$v_n = v_r + v_2 \tag{4b}$$

The state space model (3)–(4) is in the same form as that in equation (1) where the state, input and output are given as follows:

$$x = (\omega_r \quad \dot{d}_n \quad d_n \quad v_t \quad v_m)^T \tag{5}$$

$$u = (\beta \quad p)^T \tag{6}$$

$$y = (\omega_m \quad v_n)^T \tag{7}$$

Actually, it is simpler compared with equation (1) as the noise enters linearly as shown in equation (8).

$$\dot{x} = f(x,u) + n \tag{8a}$$

$$y = h(x,u) + v \tag{8b}$$

Notice that pitch and generator power are considered to be noise-free inputs. Measurement noise is associated with the measurement of rotor speed and NWS. The measurement noise $v = (v_1 \; v_2)^T$ in equation (4) is assumed white with constant diagonal covariance. Notice also that the NWS is a measurement of the relative wind v_r.

The wind model is important for the estimator and is not standard. Therefore, the description follows here in more detail. The process noise only enters the model (equation (3)) through the wind states (3c) and (3d). By using the differential equation formulation (equation (8a)), n should be interpreted as continuous time white noise corresponding to a Wiener process w as $w = \int n dt$. The 'sizes' of n and w are given by the parameter V (equation (9b)), which is the 'incremental covariance' for w in the sense that $\mathrm{Cov}(w(t_2) - w(t_1)) = V(t_2 - t_1)$. The parameters for the wind model are then given in equation (9). For more details on stochastic differential equations and Wiener processes, see, e.g., Section 10-1 of Papoulis and Unnikrisha Pillai.[19]

$$w \in W(V) \tag{9a}$$

$$V = \begin{pmatrix} V_{11}(v_m) & 0 \\ 0 & V_{22} \end{pmatrix} \tag{9b}$$

$$a(v_m) = \frac{\pi v_m}{2L} \tag{9c}$$

$$V_{11}(v_m) = \frac{\pi v_m^3 {t_i}^2}{L} \tag{9d}$$

The mean wind speed must be able to vary slowly from zero to at least 30 m s^{-1}. This is obtained with the simple random walk (equation (3d)). The incremental covariance V_{22} can be set to $\frac{2^2}{600}$ if it is assumed that the standard deviation in the change in mean wind over 10 min is 2 m s^{-1}. The turbulent wind speed dynamics (equation (3c)) is known to change with mean wind speed. This explains the mean wind speed dependent dynamics and variance via a and V_{11}. Equations (9c)

and (9d) come from requiring the same variance and 'peak frequency' for the first-order model (equation (3c)) as obtained by the Kaimal spectrum[17] in equation (10).

$$S_U(f) = \sigma_K^2 \frac{4\frac{L}{U_{10}}}{\left(1 + 6f\frac{L}{U_{10}}\right)^{\frac{5}{3}}} \Leftrightarrow \tag{10}$$

$$fS_U(f) = \sigma_K^2 \frac{f^\gamma A}{(1 + Bf^\alpha)^\beta}, \quad \alpha = 1, \quad \beta = \frac{5}{3}, \quad \gamma = 1, \quad A = 4\frac{L}{U_{10}}, \quad B = 6\frac{L}{U_{10}} \tag{11}$$

The peak frequency is here defined as the one maximizing $fS(f)$. The variance and peak frequency for the Kaimal spectrum and the first-order model is given. Notice that the peak frequencies are in Hertz and that the first part of equation (15) holds for any parameters in equation (11). From these, equations (9c) and (9d) can be derived.

$$\sigma_{v_t}^2 = \frac{V_{11}}{2\pi}\int_{-\infty}^{\infty}\left|\frac{1}{i\omega + a}\right|^2 \mathrm{d}\omega = \frac{V_{11}}{2a} \tag{12}$$

$$f_{\mathrm{p},v_t} = \frac{a}{2\pi} \tag{13}$$

$$\sigma_{\mathrm{K}}^2 = \int_{-\infty}^{\infty} S_U(\omega)\mathrm{d}\omega = (t_i v_m)^2 \tag{14}$$

$$f_{\mathrm{p,K}} = \left(B\left(\frac{\alpha\beta}{\gamma} - 1\right)\right)^{-\frac{1}{\alpha}} = \frac{v_m}{4L} \tag{15}$$

Even though the diffusion term for v_t is scaled with the state v_m, there is a small probability for negative wind speeds $v = v_m + v_t$. However, for normal turbulence intensities below 0.2, the probability is less than $2.87 \cdot 10^{-7}$ according to equation (16) where Gaussian noise is assumed. This is therefore not considered a problem for the estimation model.

$$v = v_m + v_t \tag{16a}$$

$$\mathrm{E}(v|v_m) = v_m, \quad \mathrm{V}(v|v_m) = (t_i v_m)^2 \tag{16b}$$

$$\mathrm{P}(v < 0) = \mathrm{P}(\mathrm{N}(v_m, (t_i v_m)^2) < 0) = \Phi\left(-\frac{v_m}{t_i v_m}\right) = \Phi(-t_i^{-1}) \tag{16c}$$

Notice that this wind model will add adaptivity to the estimator in the sense that it will adapt to changes in 10 min average wind speeds. If, e.g., the average wind speed increases, the turbulence time constant decreases, and the variance increases that will result in a 'faster' estimator.

2.2. Estimation procedure

The modeling discussed is in continuous time, and the model is nonlinear. Consequently, a continuous–discrete KF is used (see, e.g., Grewal and Andrews[14]). In the following, the KF for linear systems is presented first, then the modifications for nonlinear systems are given. The KF/extended KF (EKF) method is chosen because of the following merits. For a linear system with Gaussian noise, the KF gives the optimal state estimate and prediction. For non-Gaussian noise, it gives the optimal linear estimate and prediction. The EKF is known to be a good approximation to an optimal estimate for nonlinear systems.

Wind Energ. 2011; **14**:877–894 © 2011 John Wiley & Sons, Ltd.
DOI: 10.1002/we

The continuous–discrete KF

Assume the linear time varying system:

$$dx(t) = (F(t)x(t) + B(t)u(t))\,dt + dw(t) \tag{17}$$

$$y(t_k) = H(t_k)x(t_k) + D(t_k)u(t_k) + v(t_k) \tag{18}$$

$$w(t) \in W(Q(t)), \quad \mathrm{E}(v(t_i)v(t_j)^{\mathrm{T}}) = \Delta(t_i - t_j)R(t_i) \tag{19}$$

Given measurements and initial values:

$$y(t_0), y(t_1), y(t_2), \ldots, u(t), t \geq t_0 \tag{20}$$

$$\hat{x}(t_0^-) = \hat{x}_0, \quad P(t_0^-) = P_0 \tag{21}$$

Measurement update at time t_k:

$$K(t_k) = P(t_k^-)H(t_k)^{\mathrm{T}}(H(t_k)P(t_k^-)H(t_k)^{\mathrm{T}} + R(t_k))^{-1} \tag{22a}$$

$$\hat{x}(t_k^+) = \hat{x}(t_k^-) + K(t_k)(y(t_k) - H(t_k)\hat{x}(t_k^-) - D(t_k)u(t_k)) \tag{22b}$$

$$P(t_k^+) = (I - K(t_k)H(t_k))P(t_k^-)(I - K(t_k)H(t_k))^{\mathrm{T}} + K(t_k)R(t_k)K(t_k)^{\mathrm{T}} \tag{22c}$$

Time update from t_k to t_{k+1}:

$$\hat{x}(t_k) = \hat{x}(t_k^+), \quad P(t_k) = P(t_k^+) \qquad \text{(initial conditions)} \tag{23a}$$

$$\dot{\hat{x}}(t) = F(t)\hat{x}(t) + B(t)u(t) \qquad \text{(differential equation for } \hat{x}) \tag{23b}$$

$$\dot{P}(t) = F(t)P(t) + P(t)F(t)^{\mathrm{T}} + Q(t) \qquad \text{(differential equation for } P) \tag{23c}$$

$$\hat{x}(t_{k+1}^-) = \hat{x}(t_{k+1}), P(t_{k+1}^-) = P(t_{k+1}) \qquad \text{(result)} \tag{23d}$$

The continuous–discrete EKF

Assume now the nonlinear model (equation (8)). The EKF is then derived from the KF by using the following heuristic principle: use the nonlinear relations when possible and the linearization otherwise.

This means that the following are changed to use the nonlinear equations.

Measurement update at time t_k:

$$\hat{x}(t_k^+) = \hat{x}(t_k^-) + K(t_k)(y(t_k) - h(\hat{x}(t_k^-), u(t_k), t_k)) \tag{24}$$

Time update from t_k to t_{k+1}:

$$\dot{\hat{x}}(t) = f(\hat{x}(t), u(t), t) \qquad \text{(differential equation for } \hat{x}) \tag{25}$$

In all the other equations, the linearized parameters (equation (26)) must be used.

$$F(x,u,t) \triangleq \frac{\partial f(x,u,t)}{\partial x} \tag{26a}$$

$$H(x,u,t) \triangleq \frac{\partial h(x,u,t)}{\partial x} \tag{26b}$$

It is best to use the most recent values of the state estimate, i.e.,

$$H(t_k) = H(t_k, \hat{x}(t_k^-), u(t_k^-)) \tag{27}$$

$$F(t) = F(t, \hat{x}(t|t_k), u(t)) \tag{28}$$

2.3. Final estimator

To develop the EKF algorithm, it is necessary to establish the linearization, to choose an integration method, to choose/tune the initial state, covariance and possibly process and measurement covariance, and to finally check for observability and stability. A quasi-steady approximate method for an observability and stability check used here is to base the test on the time-varying linearized model. If the filter is really unstable, the computation will of course also diverge.

The linearization is in principle straightforward. The C_p and C_t functions are given as look-up tables. Derivatives of these are then implemented as look-up, i.e., interpolation in tables of numerical gradients directly obtained from the C_p and C_t tables.

The initial state was chosen close to what could be estimated by data, and the initial state prediction covariance was set from rough estimates (equation (29)).

$$\hat{x}_0 = (1.64 \quad 0 \quad 1 \quad 0 \quad 12.9)^T, \quad P_0 = \text{diag}(0.1, 0.1, 0.1, 0.1, 1)^2 \tag{29}$$

The process noise are given by the turbulence intensity and the incremental covariance for the mean wind that is chosen as follows:

$$t_i = 0.1, \quad V_{22} = \frac{2^2}{600} \tag{30}$$

The measurement noise parameters (equation (31)) are also based on sound judgement. It is assumed that the error on rotor speed is approximately 1–2% and that the uncertainty in NWS measurement is large because of blade passing and tower movements.

$$R = \text{diag}\,(0.02, 1) \tag{31}$$

The noise covariances could also be estimated. This was not carried out here partly because they can be adjusted slightly to account for the under-modeling that is needed as described below.

When testing the EKF based on the fifth-order model (equations (3)–(4)), the Kalman gain K and other related signals began to oscillate after awhile, and eventually, the values get out of range for the look-up tables. A possible reason is that the observability is too low because there is no direct measurement of tower movements. Tower movements are only seen in the NWS. This explanation is supported by the relatively high condition number of the observability matrix for the linearized system, which is around 1000.

Therefore, an EKF based on a third-order model without the tower has been tested without stability problems. The performance and testing of this EKF are seen in Figures 1–4. The data used here are 1 h data from OWEZ wind turbine WTG16 measured on 11 February 2009. As seen in Figure 1, the transient behavior and observability is satisfactory.

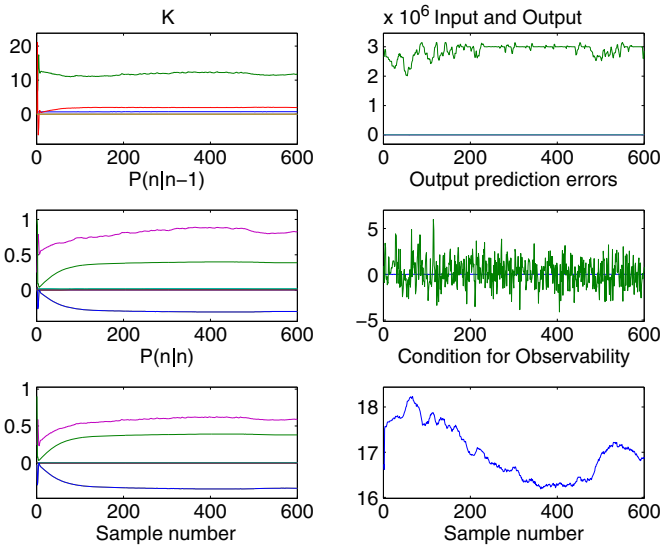

Figure 1. Transient behavior of EKF based on third-order model. The horizontal axis is Time in seconds, K is the Kalman gain and $P(n|n-1)$ and $P(n|n)$ is the state prediction and the estimation error covariance, respectively. The lower right plot is the condition number for the linearized observability matrix.

Wind Energ. 2011; **14**:877–894 © 2011 John Wiley & Sons, Ltd.
DOI: 10.1002/we

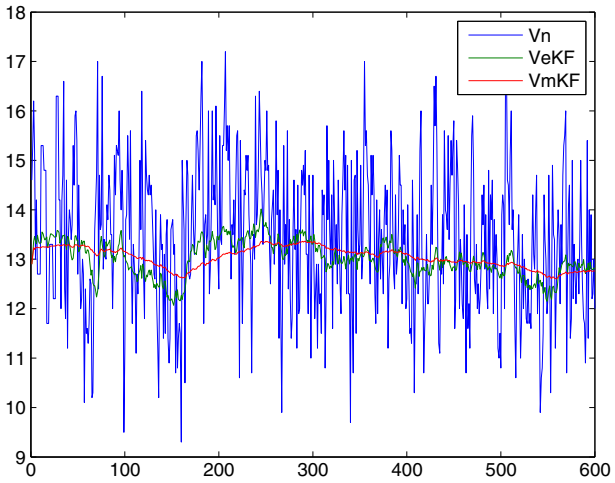

Figure 2. Comparison of nacelle wind speed and estimated effective wind speed. Vn is the measured nacelle wind speed v_n, VmKF is the estimated mean wind speed v_m and VeKF is the resulting estimated effective wind speed $v_e = v_m + v_t$. The vertical axis is in m s^{-1} and the horizontal is in seconds.

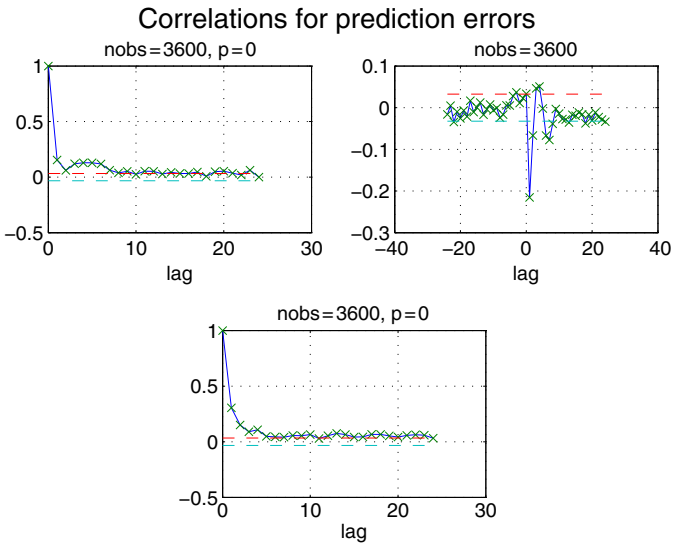

Figure 3. Residual test for the EKF based on the third-order model. The plot shows autocorrelation and cross-correlation for the output prediction errors, i.e., rotational speed and nacelle wind speed. There were 3600 samples used. p is the p-value for a portmanteau white noise test, and the dashed red and blue lines are 0.95 confidence limits for single correlations.

Comparing the NWS with the estimated ones in Figure 2 shows that the filter removes the higher frequencies; moreover, the estimates behave as expected. A portmanteau test (see Section 6.6 of Madsen[20]) with a correct model will show output prediction errors that are white noise. The model is not perfect as the tower is left out. This is the main reason for the significant correlation in the residual tests seen in Figure 3. However, these correlations are significant but acceptably small. Figure 4 shows the low-pass behavior of the system in frequency domain. The tower frequency is again hardly visible in the estimated wind but can be seen at 0.25 Hz in the nacelle wind in the lower plot.

3. FARM AND MEASUREMENTS

The ideal required measurements are stated in Table II. The meteorology mast can give free flow wind speed and direction that can be useful, but this is not crucial for this investigation. Tower and blade loadings are necessary if the models are

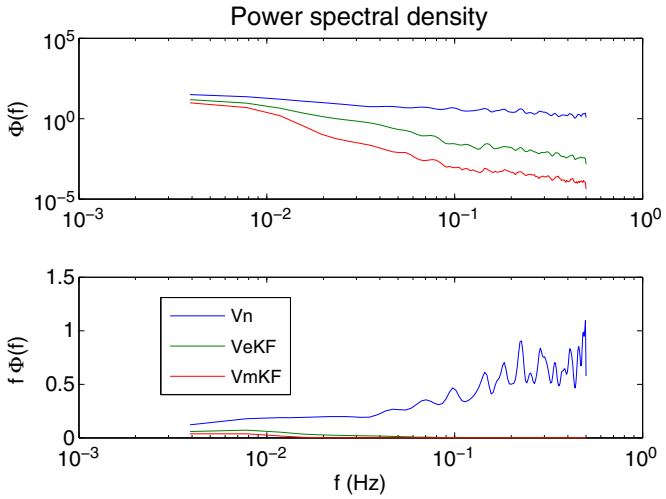

Figure 4. Spectra of nacelle wind speed and estimated effective wind speed. There 3600 samples used. The plot type with $f\Phi(f)$ versus f preferred in meteorology is also shown.

Table II. Measurement specification and available measurements from OWEZ for the six turbines WTG2-4 and WTG14-16.

General	Sample rate:1 Hz	O
	Averaging time:1 s	O
	Date / Time stamp: absolute	O
Wind turbine	Electrical power produced	O
	Electrical power reference	
	Status signal	O
	Blade pitch angles (3)	O
	Blade azimuth angle	
	Rotor speed	O
	Wind speed at turbine	O
	Wind direction at turbine	O
	Nacelle direction	O
	Tower bending moments or similar load indicators	
	Blade root bending moments or similar load indicators	
Met. mast	Wind speed at hub height	
	Wind direction at hub height	
	Temperature at 0.5, 1 and 1.5 hub height	

O, available from OWEZ.

extended to cover loading as well. Even when only focussing on wind speed, the tower bending or, e.g., tower acceleration would be a help in the estimation of EWS. For the estimation of EWS, only one common pitch angle is needed, and the power reference is not necessary.

The OWEZ farm seen in Figure 5 consists of 37 large modern V90-3MW wind turbines and all necessary parameters are available. Some drawbacks with this farm are that there are no available load measurements and the wind speed direction measurements are not aligned with north, i.e., the zero direction is unknown and different for all turbines. An approximate calibration of direction measurements is done using information from the nearby meteorological station Ijmuiden. The available signals for OWEZ are marked with a 'O' in Table II. The missing tower measurement is the biggest problem for this investigation as it was not possible to obtain observability in the estimation of EWS when including the tower in the estimation model. Consequently, the tower is excluded from the estimation model.

To illustrate some of the measurements, the most relevant signals are shown in the time domain in Figure 6 for 11 February 2009. The units used in the plot are given in Table III. Notice that the turbine goes into pause mode three times

Wind Energ. 2011; **14**:877–894 © 2011 John Wiley & Sons, Ltd.
DOI: 10.1002/we

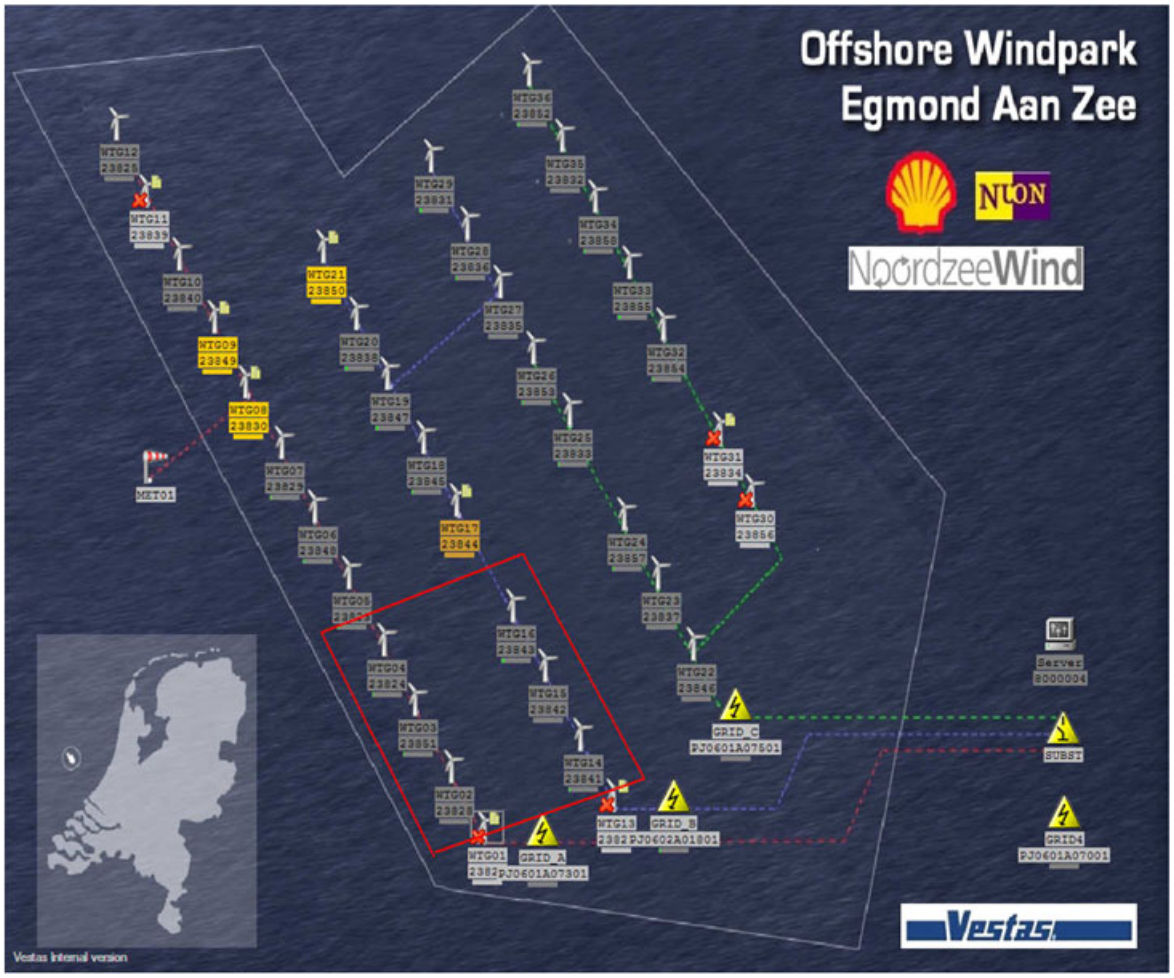

Figure 5. Layout of OWEZ. The six turbines in the red box are covered by the measurements.

at the end of the time interval. Figure 7 shows spectra for the first part of the data where the operation is close to but below rated such that the power varies with the wind speed. Notice that the tower frequency is visible in all signals except the rotor speed.

4. DATA DRIVEN MODELING RELATING WIND SPEED AT TURBINES

First, the input and the output are discussed and determined. Then the experimental conditions are described. Most of this is for convenience covered Section 3. Possible model structures will then be identified based on prior knowledge and impulse response estimates. By having a well-defined model structure, the parameters can be estimated from data, and the final model performance can be assessed. Data-driven modeling is also known as 'system identification' in Control Engineering. As general references to the methods used in the following, see Ljung[21] or Madsen.[20]

4.1. Input and output

For model development and online use of the developed model, we assume standard 1 s turbine measurements given for each turbine in the farm. The specific measurements are given in Table II for reference.

If the wind direction was fixed it might have been useful to define the measurements from upwind turbines as inputs and measurements from downwind turbines as outputs.

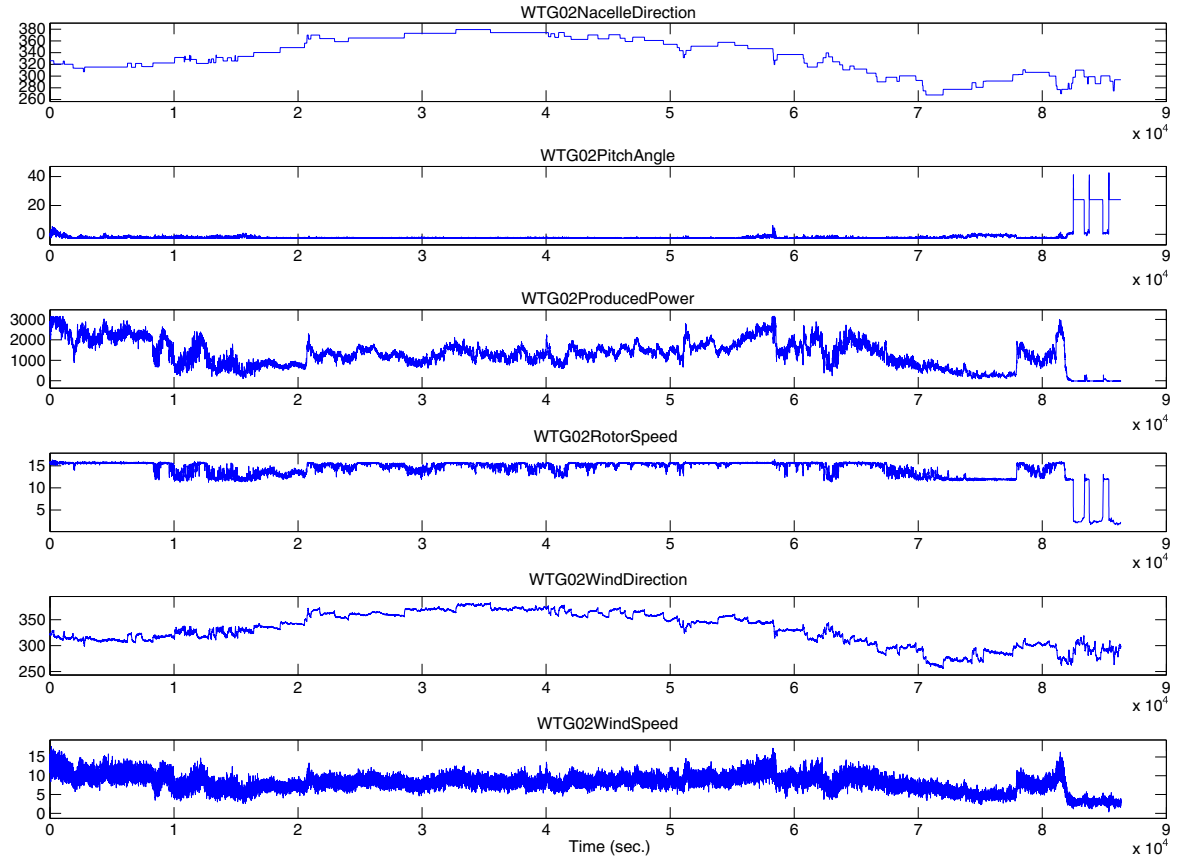

Figure 6. Time plot for signals from WT02 for 1 day, 11 February 2009.

Table III. Names and units for data in plots. For specific turbines, the names are pre-pended with WTG {turbine number}.

Name	Unit
OWEZ data	
NacelleDirection	degree
OperationalState	integer
PitchAngle	degree
ProducedPower	KW
RotorSpeed	rpm
WindDirection	degree
WindSpeed	m s^{-1}
Filtered data	
WindSpeedE	m s^{-1}

In practice, the wind direction varies continuously so no turbine is always upwind and measurements cannot be fixed as inputs or outputs. For a model valid for all wind conditions, this means that all measurements form a very large output vector, and there are no inputs. In system identification terminology, this is a multidimensional time-series model.

In this paper, a simpler model is used for a start. To this end, data where the wind direction and two turbines are approximately aligned are selected. Then the measurements on upwind and downwind turbines are input and output, respectively.

Especially for the first 3 h of the data, the average wind direction is close to 320, which is close to the direction of turbine row 4-3-2 or 16-15-14. Therefore turbine 3 will be used as input and 2 as output. Similar results were obtained using other combinations of turbines.

Wind Energ. 2011; **14**:877–894 © 2011 John Wiley & Sons, Ltd.
DOI: 10.1002/we

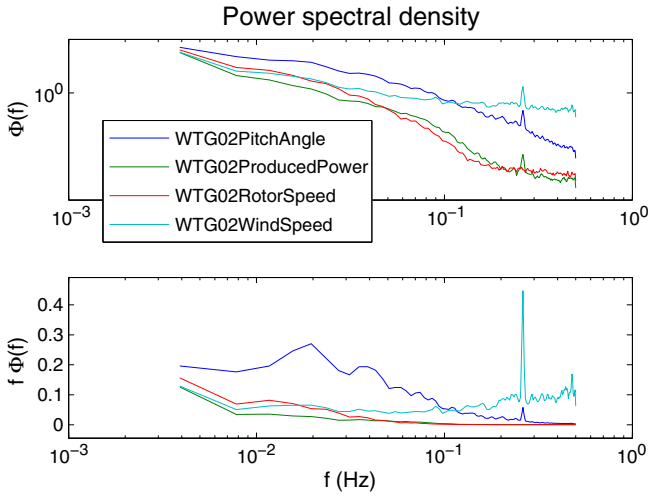

Figure 7. Power spectrum for signals from WT02. Time range $[2\ 10^3, 2\ 10^4]$, which is close to but below rated. The plot type with $f\Phi(f)$ versus f preferred in meteorology is also shown.

The wind speed in question here also needs a precise definition. Wind velocity is a vector field from $\mathbb{R}^4$ (time and space) to $\mathbb{R}^3$ (three-dimensional velocity). As the estimated models are intended for farm control, this means that the faster frequencies and smaller spatial scales, e.g., 1 m, are not relevant. The relevant wind speed is the wind speed over the rotor disc also known as the *effective wind speed*.[9,10] Light detection and ranging technique would be an option to measure EWS, but this is not part of 'standard signals from turbines', and it is also still expensive. To measure EWS, it is then necessary to use turbines as measurement devices. This is covered in Section 2. To compare with results in the literature, both point and effective wind speed will be used in this investigation. Note that it is difficult to directly compare the predictability of measured NWS and EWS as they measure different physical quantities.

4.2. Model structures

The only literature found on these specific models is Nielsen *et al.*[7] Here, an input/output (I/O) model for predicting point wind speed from measured upwind point wind speed is presented. The model included a stochastic part of ARMA type, which was not important for predictions longer than 20 s. The deterministic part has the form (32) where u_j and u_i are downwind and upwind 10 s average point wind speed measured at 80 m height at masts at Høvsøre. Further, U_{10} is the 10 min average wind speed, and d is the distance between locations. This means that the impulse response function h uses time scaling with the time it takes the average wind to move from input to output location.

$$u_j(t) = \psi_0 + \int_0^\infty h\left(\frac{U_{10}(t)}{d}s\right) u_i(t-s)\mathrm{d}s \tag{32}$$

A similar, but simpler, IO model is a good starting point for the model relating wind speed at upwind and downwind turbines.

4.3. Impulse response estimates

Initially, a nonparametric impulse response is estimated to indicate the type of model needed and to test the delay model idea coming from the physical interpretation that the turbulence travels downwind as it decays.

The nonparametric impulse response estimate in Figure 8 is for EWS based on the first 8 h. There is a significant 'hump' centered around 80, which multiplied by average upwind EWS gives 733 m under the given wind conditions that is somewhat larger than the inter-turbine distance of 632 m. However, the average upwind EWS corresponds to free/undisturbed wind that is larger than the actual wind in the farm, and this explains most of the mismatch. Nevertheless, this supports the existence of a delay. It has been tried to focus on shorter time intervals with varying wind speeds to test if the delay approximately equals the time it takes the mean wind to travel between turbines. However, reducing to, e.g., 2 h makes almost all estimates insignificant. Furthermore, the impulse response estimate for NWS was generally insignificant.

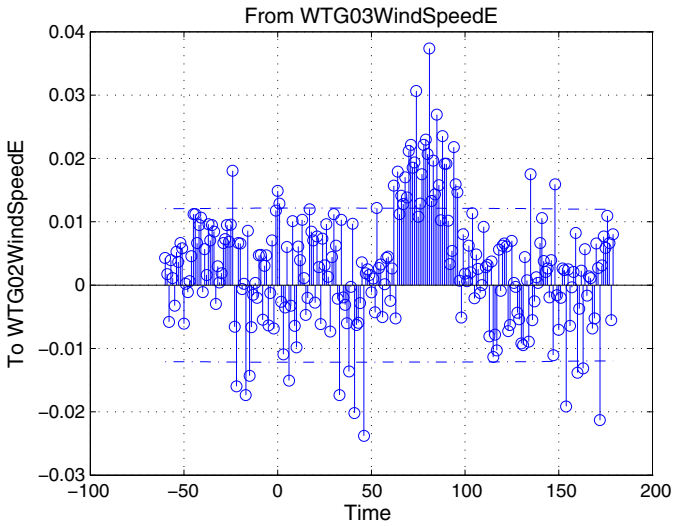

Figure 8. Nonparametric impulse response estimate for EWS. Data: 11 February 2009; WT3 to WT2, first 8 h; average wind, 9.17 m s^{-1}. The dash-dotted lines are 0.95 significance limits.

4.4. Simple linear time-invariant (LTI) models

In this section, standard LTI models are described. Then the parameters are estimated, and the corresponding 1, 30 and 60 s forecast errors are calculated.

For single-input single-output (SISO) system, an LTI model can be defined as in equation (33). Here, the output y is a sum of filtered input u and filtered white noise e. The transfer functions G and H are defined using the 'back step operator' q^{-1} formulation. For more details, see, e.g., Ljung.[21]

$$y(t) = G(q^{-1})u(t - n_k) + H(q^{-1})e(t), \quad e(t) \in \mathrm{ID}(0, \sigma^2) \tag{33a}$$

$$G(q^{-1}) = \frac{B(q^{-1})}{A(q^{-1})F(q^{-1})}, \quad H(q^{-1}) = \frac{C(q^{-1})}{A(q^{-1})D(q^{-1})} \tag{33b}$$

$$A(q^{-1}) = 1 + a_1 q^{-1} + \cdots + a_{n_a} q^{-n_a} = \sum_{i=0}^{n_a} a_i q^{-i}, \quad a_0 = 1 \tag{33c}$$

$$B(q^{-1}) = \sum_{i=0}^{n_b} b_i q^{-i}, \quad C(q^{-1}) = \sum_{i=0}^{n_c} c_i q^{-i}, \quad c_0 = 1 \tag{33d}$$

$$D(q^{-1}) = \sum_{i=0}^{n_d} d_i q^{-i}, \quad d_0 = 1, \quad F(q^{-1}) = \sum_{i=0}^{n_f} f_i q^{-i}, \quad f_0 = 1 \tag{33e}$$

This model structure is the most general one among LTI SISO I/O models. To define a specific model structure in this class, the structural parameters $n_a, n_b, n_c, n_d, n_f, n_k$ must be chosen. This investigation should reveal if there is any potential for predicting EWS. Therefore, the following simplifying choices have been made. Autoregressive exogenous (ARX) models where $C = D = F = 1$ were tested because they give a unique parameter estimate and are fast and robust. In case of under modeling, standard prediction error methods for ARX structures can give bias for the lower frequencies that could give bad performance for long-term prediction. This would then be fixed with an output error (OE) structure where $A = C = D = 1 \Rightarrow H = 1$ or a Box–Jenkins (BJ) structure where H has separate parameters, i.e., $A = 1$. As the impulse response estimate indicates a delay larger than 50 samples, also models with delay are tested. Test not shown here indicate

Wind Energ. 2011; **14**:877–894 © 2011 John Wiley & Sons, Ltd.
DOI: 10.1002/we

optimal delays $n_k \geq 60$, typically 70; therefore, $n_k = 60$ has been chosen as the input needed for prediction and is then known up to prediction horizons of 60 s. A model order of 2 is used for all model structures discussed previously. The reasons are that second-order models can reproduce the 'bump' like impulse response, and there seems to be no substantial improvement from using higher-order models. To compare with what can be obtained without upwind information, an autoregressive (AR) structure where $B = 0 \Rightarrow G = 0$ and $C = D = 1$ is included as well as the special AR structure $A(q^{-1}) = 1 - q^{-1}$ known as the persistence method where any prediction always equals the last measurement.

For estimation, the first 4 h are used, and for cross validation, the next 4 h are used as illustrated in Figure 9.

The most important results are shown in Table IV. The root-mean-square (RMS) error is the standard prediction error estimate (equation (34)). The fit (35) shows how much of the standard deviation in the output is explained by the model.

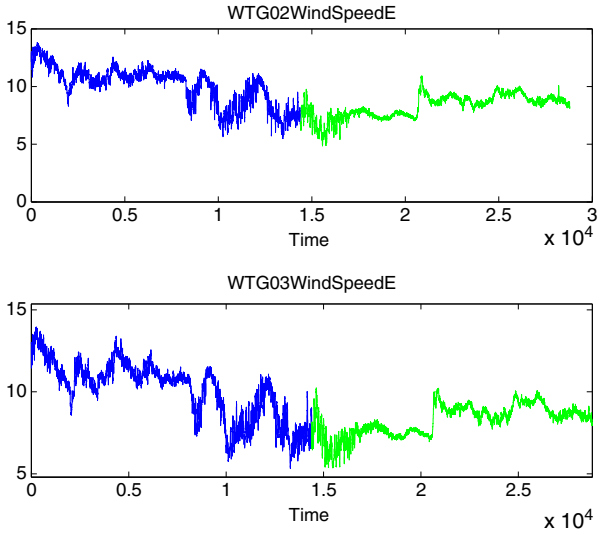

Figure 9. Data to estimate LTI models. First 4 h for estimation, last 4 h for cross-validation. Data: 11 February 2009.

Table IV. Predictability for nacelle wind speed using one upwind turbines and LTI models.

Type	OE	ARX	ARXDel	BJDel	AR	Per
n_a	0	2	2	0	2	1
n_b	2	2	2	2	—	—
n_c	0	0	0	2	0	0
n_d	0	0	0	2	0	0
n_f	2	0	0	2	—	—
n_k	0	0	60	60	—	—
Prediction horizon (s)			Fit (%)			
1	32.149	37.441	37.558	42.233	34.412	28.535
30	32.149	21.955	23.943	32.062	−10.935	9.159
60	32.149	21.933	23.937	31.548	−63.183	6.071
∞	32.149	21.933	23.937	32.153		
Prediction horizon (s)			RMS (m s^{-1})			
1	0.886	0.817	0.816	0.755	0.857	0.934
30	0.886	1.020	0.994	0.888	1.449	1.187
60	0.886	1.020	0.994	0.894	2.132	1.227
∞	0.886	1.020	0.994	0.886		

The columns in the two bottom sections, Fit and RMS, hold the results using the model structure specified in the column in the top section. The model structures marked with 'Del' includes the 60 s delay. Prediction horizon ∞ corresponds to pure simulation. The negative fit values are due to under-modeling, given bias when parameters are optimized for one step prediction and then used for multistep prediction.

$$\mathrm{RMS} = \sqrt{\frac{1}{N}\sum_{t=1}^{N}(y(t) - \hat{y}(t|t-k))^2} \tag{34}$$

$$\mathrm{Fit} = 1 - \frac{\mathrm{RMS}}{\hat{\sigma}_y} \tag{35}$$

As seen, the maximal fit for 60 s predictions for NWS is less than 1/3 corresponding to a RMS error of 0.9 m s^{-1}, which is a poor fit. It is obtained with the OE model structure. Even though this is poor, it is far better than that of persistence, which gives a fit of 0.06. The rows marked with ∞ are the results from a prediction horizon at infinity meaning that no old outputs are used, only inputs are used to calculate the output, this in turn is also called pure simulation. Notice that the results are nearly the same as for a prediction horizon at 30 s or more. This means that the stochastic part does not really play a role for variations over 30 s.

For the EWS, the results are shown in Table V. The best results are obtained using 60 s delay and the ARX or BJ model, which for a minute prediction gives an RMS error of 0.33 m s^{-1} corresponding to a 95% significance limits at $\pm$0.66 m s^{-1}, which is small enough to be useful. The results in Nielsen *et al.*[7] for this mean wind speed, which is 8.3 m s^{-1} for the validation data, give a significance interval of $\pm$0.6 m s^{-1} but for point wind speed only separated by 300 m. Again, this is difficult to compare, but at least, there is no clear conflict. Comparing the ARX structure with the persistence method shows that the prediction error of the former is close to 0.7 of the latter.

The last column in Table V is the results where the ARX structure is used, but the input is now from turbine 4 that is approximately at double the distance, i.e., 1277 m compared with that of turbine 3, which is 632 m from turbine 2. The delay is therefore doubled to $n_k = 120$. It is interesting to see that even at this distance, the 1 min prediction error is reduced to approximately 0.82 compared to persistence. For EWS, the stochastic part is seen to play a slightly bigger role. Still, it does not improve the 1 min prediction much over pure simulation.

To give some visual results, Figure 10 zooms in on one of the large gusts in the validation data. Here, it is clearly seen that a simple prediction model based on the first or second upwind turbine outperforms the persistence method.

4.5. Alternative model structures

For validation, other combinations of wind direction with aligned turbines were tested, e.g., WTG3-4 in Figure 5. Most of them gave similar results as the ones shown here for WTG2-3. Also, it was tested if the prediction performance was improve from including more turbines, e.g., using WTG3, 13 and 14 to predict WTG2. However, this did not improve performance. Another immediate idea is to include the wind speed direction relative to the direction between turbines. As the direction is definitely not expected to enter linearly in the model, nonlinear model structures as, e.g., nonlinear ARX models and Hammerstein models[21] have been tested. It was not possible to improve on the linear models. The only one that looked promising was the Hammerstein model where the upwind EWS enters linearly and the relative wind direction enters via a piecewise affine input nonlinearity. The estimated static input nonlinearity is shown in Figure 11. Here, it is seen that the predicted wind speed downwind decreases when the wind direction is closer to the turbine directions; notice also that there seems to be a bias in the calibration as the input nonlinearity is not an even function.

Table V. Predictability for effective wind speed using one upwind turbine and LTI models.

Type	OE	ARX	ARXDel	BJDel	AR	Per	ARXDel4To2
Prediction horizon (s)				Fit (%)			
1	60.008	94.444	94.466	94.520	94.430	94.380	94.454
30	60.008	63.515	68.346	67.928	59.458	59.516	64.846
60	60.008	60.958	66.862	66.056	52.253	52.501	61.178
∞	60.008	62.698	65.208	65.736			55.140
Predicate horizon (s)				RMS (m s^{-1})			
1	0.397	0.055	0.055	0.054	0.055	0.056	0.055
30	0.397	0.362	0.314	0.318	0.403	0.402	0.349
60	0.397	0.388	0.329	0.337	0.474	0.472	0.386
∞	0.397	0.370	0.345	0.340			0.445

Wind Energ. 2011; **14**:877–894 © 2011 John Wiley & Sons, Ltd.
DOI: 10.1002/we

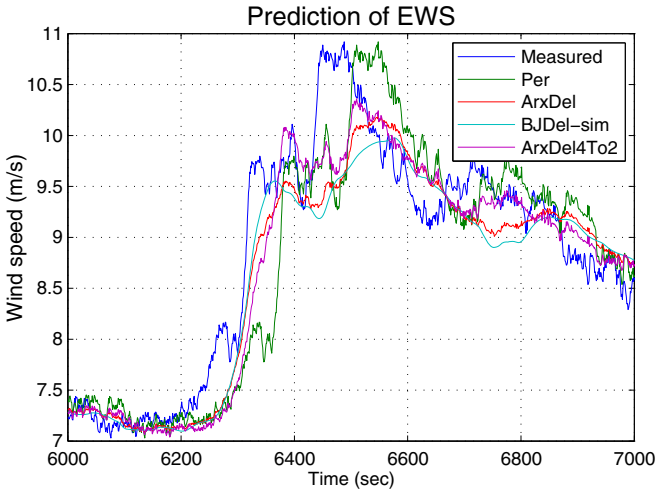

Figure 10. Example of predictions with a gust. Legend: 'Measured' simply is the measured EWS on the downwind turbine WT2. The rest of the curves 'Per', etc., are 1 min predictions except BJDel-sim that is pure simulation. See the text for further details. Data: 11 February 2009.

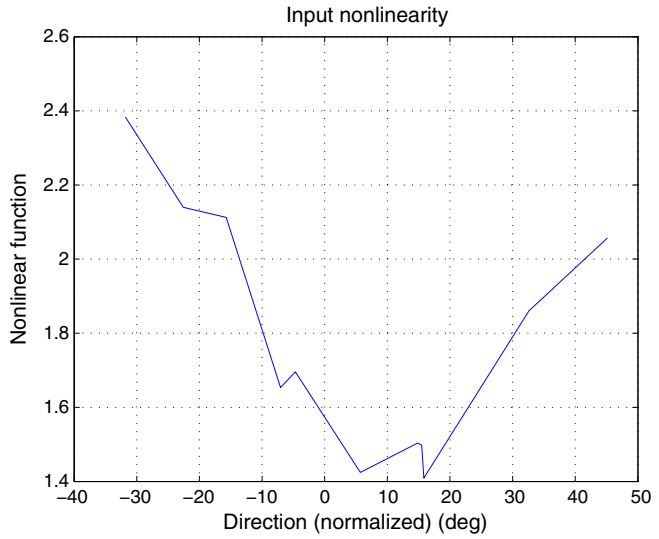

Figure 11. Hammerstein input nonlinearity for wind direction. Data: 11 February 2009.

5. CONCLUSION

In this paper, an estimator for effective wind speed was developed. This estimator includes the wind speed in a new more accurate way compared with the estimators found in the literature. By using the estimator, the effective wind speeds for six turbines in the OWEZ farm have been estimated. These effective wind speeds are then used for developing models with the purpose of predicting wind speed for a turbine up to 1 min ahead using standard measurements from an upwind turbine. Based on simple classical models, the prediction error for this effective wind speed can be reduced by 30% using an upwind turbine compared with the persistence method. This reduction is for a prediction horizon of 1 mine and a distance of 632 m. The smallest standard deviation for this prediction error is 0.33 m s^{-1} corresponding to a 95% confidence interval at ± 0.66 m s^{-1}, which is sufficiently small to be useful. When the distance is approximately doubled to 1277 m, the reduction falls from 30% to approximately 15%.

ACKNOWLEDGEMENTS

This work is supported by the EU project Aeolus under contract number 224548 and by the project CASED founded by Danish Agency for Science Technology and Innovation.

REFERENCES

1. Gjengedal T. Large-scale wind power farms as power plants. *Wind Energy* 2005: 361–373.
2. Bjerge C, Kristoffersen JR. Run an offshore wind farm like a power plant. *VGB PowerTech* 2007; **87**: 63–66. ISBN 1435-3199.
3. Maciejowski JM. *Predictive Control with Constraints*. Prentice Hall, 2002.
4. Findeisen R, Imsland L, Allgower F, Foss BA. State and output feedback nonlinear model predictive control: an overview. *European Journal of Control* 2003; **9**: 190–206.
5. Zhao R, Su Y, Knudsen T, Bak T, Shen W. Multi-agent model for fatigue control in large offshore wind farm. In *2008 International Conference on Computational Intelligence and Security (CIS'08)*; 71–75. IEEE, IEEE Computer Society, 2008. ISBN 978-0-7695-3508-1. DOI:10.1109.
6. Sørensen P, Hansen AD, Thomsen K, Buhl T, Morthorst PE, Nielsen LH, Iov F, Blaabjerg F, Nielsen HA, Madsen H, Donovane MH. Operation and control of large wind turbines and wind farms - final report, Technical Report Risø-R-1532(EN), Risø, 2005.
7. Nielsen HA, Madsen H, Sørensen P. Ultrashort term wind speed forecasting. In *European Wind Energy Conference & Exhibition, London, November 2004. EWEA*, EWEA, 2004.
8. Panofsky HA, Dutton JA. *Atmospheric Turbulence*. John Wiley & Sons, 1984.
9. Østergaard KZ, Brath P, Stoustrup J. Estimation of effective wind speed. In *Journal of Physics: Conference Series 75*, EWEA, IOP Publishing, 2007.
10. Leithead WE. Effective wind speed models for simple wind turbine simulations. In *BWEA 1992*, 1992; 321–326.
11. Van der Hooft EL, Van Engelen TG. Estimated wind speed feed forward control for wind turbine operation optimization. In *European Wind Energy Conference, London*, ECN, 2004. ECN-RX–04-126.
12. Odgaard PF, Damgaard C, Nielsen R. On-line estimation of wind turbine power coefficients using unknown input observers. In *17th IFAC World Congress*, IFAC, IFAC, 2008; 10646–10651.
13. Qiao W, Zhou W, Aller JM, Harley RG. Wind speed estimation based sensorless output maximization control for a wind turbine driving a dfig. *IEEE Transactions on Power Electronics* 2008; **23**(3): 1156–1169.
14. Grewal MS, Andrews AP. *Kalman Filtering*, 2nd edn. Prentice Hall, Inc., 2001.
15. Egmond aan zee offshore wind farm. [Online]. Available: http://www.noordzeewind.nl/ (Accessed December 2009).
16. Snel H, Schepers JG. Engineering moles for dynamic inflow phenomena. *Journal of Wind Engineering and Industrial Aerodynamics* 1992; **39**: 267–281. The title says "moles" but the authors meant "models".
17. Burton T, Sharpe D, Jenkins N, Bossanyi E. *Wind Energy Handbook*. John Wiley, 2008.
18. Munteanu I, Bratcu AI, Cutululis N-A, Ceanga E. *Optimal Control of Wind Energy Systems*. Springer, 2008.
19. Papoulis A, Unnikrisha Pillai S. *Probability, Random Variables and Stochastic Processes*, 4th edn. McGraw-Hill, 2002.
20. Madsen H. *Time Series Analysis*. Chapman & Hall, 2008. ISBN: 978-1-4200-5967-0.
21. Ljung L. *System Identification, Theory for the User*, 2nd edn. Prentice-Hall information and system sciences series. Prentice-Hall, 1999.